Available online at www.scientiaresearchlibrary.com

Scientia Research Library

ISSN 2348-0416
USA CODEN: JASRHB

Journal of Applied Science And Research, 2014, 2 (1):175-189
(*http://www.scientiaresearchlibrary.com/arhcive.php*)

Flow-bed interactions analysis and application of automatic close range digital photogrammetric survey in a laboratory flume

Donatella Termini[1], Mauro Lo Brutto[2]

Dept. of Civil, Environmental, Aerospace and Materials Engineering, University of Palermo, Italy

ABSTARCT

This paper reports on a laboratory study in which the automatic digital photogrammetric survey was applied to derive the high-resolution Digital Surface Model (DSM) of the bed topography, used for the flow-bed interactions analysis, in a large amplitude meandering laboratory flume. The analysis has been conducted with the aid of detailed data of three-dimensional flow field previously collected using the acoustic Doppler velocity profiler DOP2000. The applied surveying procedure has allowed the evaluation of the DSM with a resolution of ±0.5 mm. The detailed DSM has been compared with peculiar maps describing the flow velocity pattern (downstream and the cross-stream flows) and the shear velocity distribution along the meandering flume. The comparison has highlighted that high quality topographic data are of crucial importance to evaluate the cross-circulation effect on the redistribution of the velocity and boundary shear stress and, thereby, on the meandering channel evolution.

Keywords: meandering channels; bed topography; erosion; flow pattern; laboratory flumes; close range photogrammetry

INTRODUCTION

As it is well known, in nature, different meandering streams exhibit different geometric characteristics and/or the stream conditions may vary from one meander loop to another (da Silva et al., 2006). In fact, many laboratory and field studies (among others Hooke, 1975; Bridge and Jarvis, 1976; Chang, 1988; Whiting and Dietrich, 1993) and numerical researches (see as an example Termini and Yalin, 2004), show that the evolution of meander wave is mainly governed by the bed deformation that drives the erosion process at the channel banks. Particularly, outer-banks are considerably vulnerable to erosion processes.

Bed topography is mainly shaped by the bed shear stress distribution (see as an example Hooke, 1975; Whiting and Dietrich, 1993), which is determined by the distribution of downstream flow velocity. Recent researches (see as an example Blanckaert and Graf, 2004; Blanckaert et al., 2008; Termini and Piraino, 2011) highlight that the distribution of downstream flow velocity especially

depends on two factors: 1) the bed topography itself; 2) the advective transport of downstream momentum by the cross-stream flow (i.e. the flow perpendicular to channel axis), determined as effect of the channel curvature. Particularly, in curved narrow streams, the advective momentum transfer especially contributes to the outward shift of the downstream flow velocity.

Furthermore, many theoretical predicting models have been developed to describe the complex interplay flow pattern - bed deformation. But, most of them are based on simplified working hypothesis and set of equations (among others Odgaard, 1981; Dietrich and Smith, 1983; Whiting and Dietrich, 1991). In recent years, because of the growing interest and attention given to three-dimensional flow structures and the advances in computational power, three-dimensional predictive numerical models have been also developed (see as an example Wilson et al. 2003; Olesen, 2003). The application of such a sophisticated numerical models have farther highlighted the importance of high quality bed topography data in predicting complex morphological processes (Rumsby et al. 2008). Conceptual models, based on the field observations of the evolution of natural channels, have been also elaborated by some geomorphologists (as an example Hickin and Nanson, 1984; Hooke, 2003). But also the quantification of geomorphologic consequences of fluvial system changes (locations changes, sediment budgets, sediment trjectories,..) requires knowledge of high resolution topographic data (Lane et al., 2003).

However, because of the difficulty in acquiring accurate spatial resolution data in rivers, the validation of forecasting models and/or the testing of protective techniques of bank erosion have been usually conducted in laboratory flumes. Based on the fact that the time scale of the bank deformation is usually much larger than that of the bed deformation (Yalin, 1992; Binns and da Silva, 2009) the flow-bed interactions have been generally analyzed by ignoring the bank deformability. Thus, the major part of studies have been conducted in laboratory flumes with fixed banks (among others Hooke, 1975; Whiting and Dietrich, 1993; Blanckaert and Graf, 2001; Zolezzi et al., 2005; da Silva et al., 2006; Termini, 2009). The behaviour pattern of the meander wave has been predicted focusing on the equilibrium bed deformation (among others Struiskma et al., 1985; Zolezzi et al., 2005; Lanzoni and Seminara, 2006; da Silva et al., 2006; Termini, 2009), which may be controlled by the upstream and/or downstream boundary conditions of the channel reach examined (Zolezzi et al, 2005; Lanzoni and Seminara, 2006), and on its effect on the bank erosion (i.e. upstream or downstrem skewed shape of the meander wave– see in Seminara et al., 2001). Particularly, studies carried out in large amplitude meandering channels (Whiting and Dietrich, 1993; Seminara et al., 2001; Termini, 2009) have highlighted that the bed topography is the combination of the steady point bar-pool bed configuration and of migrating large scale bed forms superimposed over it. Both these morphodynamic features might also be of crucial interest for the prediction of the evolution of the meander wave, because they could opportunely drive bank erosion, as in low amplitude meandering channels (Yamaoka and Hasegawa, 1983). From the aforementioned it is clear the increasing need for high resolution topographic data to better model fluvial systems and to conduct geomorphological analyses. The point is that, especially to investigate the time variation of the aforementioned processes, fast and accurate devices are needed. Moreover, high quality topographic data with fast surveying procedure is more difficult to obtain with spatially complex surfaces. As highlighted by Lane et al. (2003), automation of surveying procedures, coupled with softwares for processing and visualization of large data sets, would allow the high resolution topographic representation and, thus, the quantification of morphological changes and improvements in the prediction of flow processes in 3D numerical models.

Different techniques have been applied to measure the bed topography in laboratory flumes. Some researchers (see as an example Whiting and Dietrich, 1993; Binns and da Silva, 2009) measured the

bed profile in specific cross sections, opportunely selected along the channel, by using a vertical graduated steel rod clamped on a horizontal bar. Such a method is very simple to use but it presents many limitations: it needs long measurement times, it is not accurate, it is not automatic and it does not allow the repeatability of the measure.

Other measurement tools, based on servo-controlled vertical profilers, have been also used especially for laboratory applications (see as an example Friedrichs and Graf, 2006; Termini, 2009). Some of such devices are based on electric conductibility of water (Palma et al., 2010); others are based on laser technologies (see as an example in Zolezzi et al, 2005; Cochrame and Flanagan, 2006). The first type has the capability to work very close to the bed of the flume without effective contact and it allows the dynamic surveying of the bed surface also in the presence of water (as an example, the PV-09 by Delft Hydraulics); the second type requires a dry surface so that it needs the stopping of experimental runs at specific intervals of time. Both of them are accurate (precision variable in the range 0.1 – 1. mm) and are quite simple to use, but they present some disadvantages: the measurement times are as long as high is the level of detail required (three-dimensional points along bed profiles are obtained as result of measurements); in order to automate the surveying procedure they require a motorised positioning system to drive the vertical sensor on the plan; it is necessary to interpolate the measured profiles to obtain the bed topography.

Close range digital photogrammetry have provided a more powerful tool to rapidly and automatically measure bed surface in laboratory channels (Chandler et. al., 2001; Rieke-Zapp and Nearing, 2005; Abd-Elrahman and Gad-Elraab, 2008; Gessese et al., 2010; Heng et al., 2010).

The major advantages of the close range digital photogrammetry are related to the fact that it can be scaled according to the project requirements (Rieke-Zapp et al., 2001) and that the camera is easy to handle. Furthermore, the use of non-metric digital cameras (Chandler et. al., 2005) and of many commercial softwares allows the photogrammetric survey to obtain a high level of details avoiding expensive investments in equipment.

More recently, laser scanning technology has allowed the acquisition of 3D data with a very high level of details and automation. In fact, the application of Terrestrial Laser Scanning (TLS) systems is becoming more and more frequent in geomorphology, especially for medium-scale and small-scale studies (Rumsby et al., 2008). The TLS systems allow the acquisition of 3D data with many advantages (very high level of details, accuracy, automation and scanning speed) but they still have high costs.

For large-scale applications (as well as in laboratory flumes) the use of digital photogrammetry is still today preferred (Heng et al., 2010). In comparison with the TLS systems, the photogrammetric systems permit to have a more rapid data acquisition, a more flexible camera-to-object distance and a wider vertical range of the investigated surface (Rieke-Zapp and Nearing, 2005).

In this context, this paper concerns high resolution bed topographic surveying and representation to investigate the three-dimensional morphology and its effect on the flow pattern in a large amplitude laboratory meandering flume. The two main research objectives of the work are: 1) to verify the applicability of close-range digital photogrammetric survey to accurately measure such a spatially complex bed surface; 2) to examine (with the aid of the measured bed surface and of detailed flow velocity data) how the accurate measure of the bed surface improves the prediction of flow-bed-banks interaction processes. For this purpose, it is verified how the localization of the erosion zones are related to flow velocity and bed shear stress distributions along the channel.

The data have been collected in a meandering flume constructed at the Hydraulic laboratory of Dipartimento di Ingegneria Civile, Ambientale ed Aereospaziale - University of Palermo – Italy. The DSM (Digital Surface Model) of the bed, surveyed by the “typical” close range photogrammetric work-flow (camera calibration, interactive image orientation and 3D scene restitution) technique, is compared with peculiar maps showing the flow pattern and the bed shear

stress distribution along the meander wave. Because of the complex plane shape of the channel, a large number of images (more than 300) have been acquired. The applied surveying procedure has allowed the attainment of a good compromise between the high accuracy (±0.5 mm) of the photogrammetric measurements and the surveying time required for the application.

MATERIAL AND METHOD

The experimental data were collected in a large amplitude meandering flume that follows a sine-generated curve (Langbein and Leopold, 1966) with a deflection angle of 110°. In fact, following), the sine-generated function well approximates the shape of real meanders. The channel is constructed upon a concrete basement large enough to accommodate two meander wavelengths. In agreement with the conditions observed in natural stream (see also in Yalin and da Silva, 2001 p. 83), it can be supposed that the flow width, *B*, does not vary in any systematic manner in the flow direction and that it is related to the meander wavelength, Λ_m, as $\Lambda_m \cong 2\pi B$ (Yalin, 1992). The channel cross section is rectangular (width B=0.50 m). The axis of the meandering flume is almost 27 m long (Figure 1).

The experimental apparatus and the flow measurement conditions were presented in details in previous works (Termini, 2009; Termini and Piraino, 2011) and, thus, only some peculiar features are summarized herein; more details on photogrammetric survey procedure are given in this work. The equilibrium bed topography was obtained at the end of a mobile-bed run carried out with flow discharge Q=0.012 m^3/s, initial longitudinal centreline bed slope S=0.371%, initial channel-averaged flow depth h=5.2 cm. The establishment of the equilibrium bed configuration was checked as discussed in Termini (2009). The equilibrium bed surface was then measured by the help of the 3D automatic position system opportunely fixed at the concrete basement of the channel (see Figure 2a). The position system includes two subsystems: the mechanical movements subsystem; the command and control subsystem. The mechanical movement subsystem consists of two units of high-precision movement in the orthogonal directions x and y (6.0 m long) and of one vertical unit allowing a movement of high-precision of 1.1 m. The movements are made by DC servo feedback with tachometer for speed and encoder for position. To allow the limitation of the work area, the end positions are controlled by means of movable mechanical switches. The handling units described above are mounted above a support structure consisting of complete frame with 6 legs, adjustable in height, consisting of beams IPE 160. The command and control subsystem (Figure 2c) consists of a personal computer standard PXI by National Instruments s.r.l., running on Win 2000, for the control and command of the handling device. This subsystem includes the control board, 4 PXI boards, the capture card, the cabinet containing the power drivers for motors, the protective devices, the devices for automatic control. The system uses the language of LabView for control applications.

EQUILIBRIUM BED TOPOGRAPHY BY PHOTOGRAMMETRIC SURVEY

Methods

Following previous geomorphologic applications (Chandler et al. 2003; Chandler et al. 2005; Rieke-Zapp et al., 2001; Wackrow et al., 2007; Heng et al., 2010), the equilibrium bed surface was measured by a photogrammetric survey using a non–metric digital camera. In particular, a Nikon D80 digital camera equipped with a 28 mm Nikkor f/2.8 D fixed focus lens was used. The sensor was CCD with a sensor size of 23.6 mm x 15.8 mm, a pixel size of 6.1 μm and an effective resolution of 3872 pixels×2592 pixels.

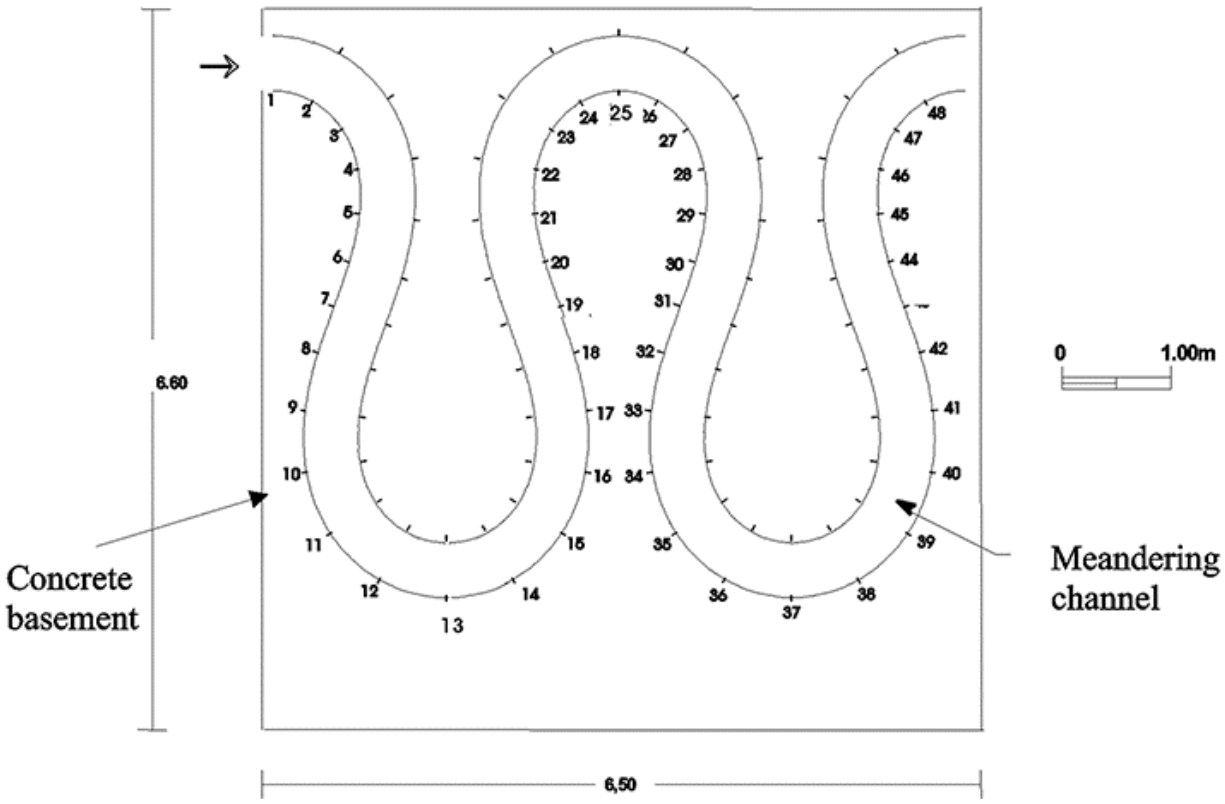

Figure 1. Plane view of the meandering channel

The photogrammetric block geometry was chosen in order to obtain: 1) high accuracy of photogrammetric measurements (3D accuracy of ±0.5 mm, being D_{50}=0.65 mm) compatibly with the physical constraints and the complex plane-shape of the channel; 2) simpleness, rapidity and repeatability of the photogrammetric survey.

On the basis of the aforementioned, the digital camera was firmly mounted on the 3D automatic position system (Figure 2b), so to obtain the average camera-to-object distance of 0.67 m from the bed surface and the automatic movement of the camera. In fact, the camera moved automatically (through the PXI computer) along the channel axis trajectory and the photogrammetric coverage could be repeated several times using the same project. By taking into account the camera-to-object distance (0.67 cm), the theoretical accuracy was of ±0.34 mm (Krauss, 1999), that is compatible with the accuracy of photogrammetric measurements required; the image scale was 1/24 and the coverage of each image was about 56.5 cm ×37.8 cm. Because the focal length of camera was of 28 mm, each pixel was equal to 0.15 mm in the object space.

A stereoscopic coverage was planned for the whole meandering flume (Figure 3). The photogrammetric strips were selected providing an end lap of 90% for the first two and the last two images of each strip and of 70% for the other images along the strip. Such difference in overlap was chosen on the basis of preliminary tests which showed that, because of the construction characteristics of the channel (especially the height and the slightly deformation of the banks), the acquisition of the areas near the banks was particularly difficult. The side lap was set equal to 30%. In order to avoid changes of the camera focal length, the lens were blocked with tape.

The main disadvantage of this approach is the high number of images needed to coverage the whole channel. The number of images was equal to 360, divided into 68 strips. The acquisition time of the

images was approximately equal to 2 hours, which can be considered short taking into account the large number of images acquired.

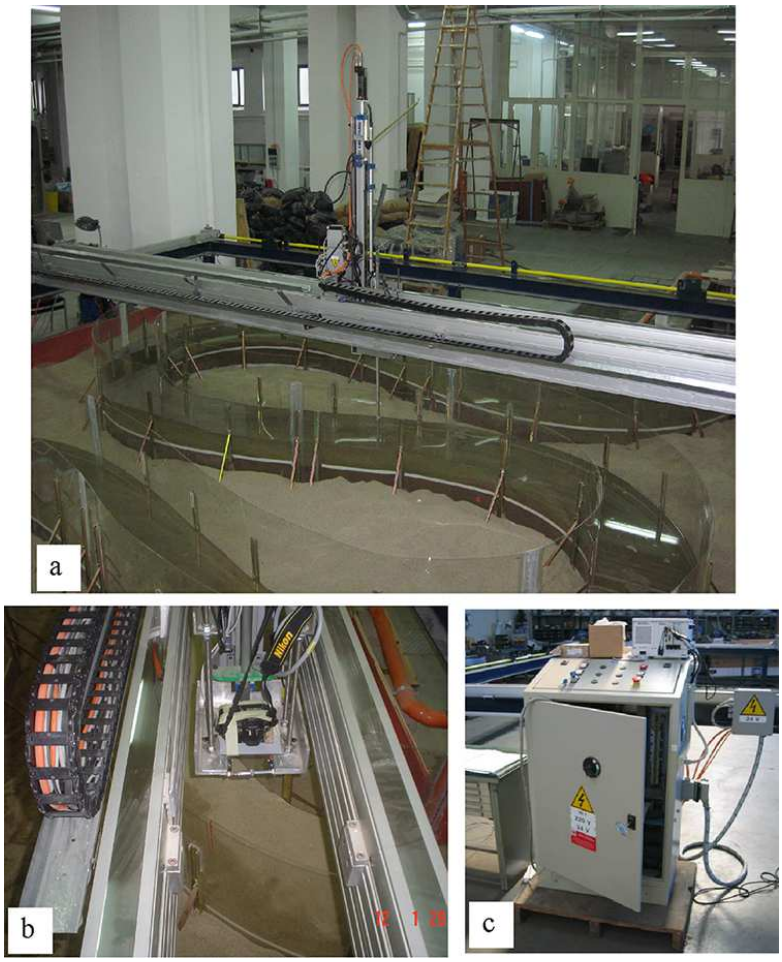

Figure 2. a) Lateral view of automatic positioning system; b) support of digital camera; c) command and control subsystem

Results and Discussion

The camera calibration was performed by using two commercial softwares: Image Master Calib (Topcon, 2010a) and iWitness (PhotoMetrix, 2006). The camera calibration was carried out through the Image Master Calib package by considering the 2D calibration sheet printed with a size of 29 cm×42 cm. The images of the calibration sheet were taken both from the five Image Master Calib standard positions (direct front, upper location, lower location, left side and right side) (Topcon, 2010a) and from other four positions (two other images from left and right side, two frontal images with the camera rotated respectively +90 ° and -90 °). In fact, according with Remondino and Fraser (2006), a planar object point array can be employed for camera calibration if the images are acquired with orthogonal roll angles, a high degree of convergence and, desirably, varying object distances. Then, the camera calibration was repeated with iWitness package by using the fully automatic camera calibration process and the twelve colour coded targets available as accessory for iWitness (PhotoMetrix, 2006). The target were positioned to form a 3D testfield. Twenty-three images were taken from different distances with a high degree of convergence and with orthogonal roll angles.

Two different sets of camera calibration parameters were computed. Finally, the datasets obtained by applying the two packages were compared. Table 1 reports the values of calibration parameters (i.e. the principal distance *c*, the principal point offset -*xp* and *yp*- the coefficient of the radial - *K1, K2, K3*- and the tangential lens distortions - *P1, P2*) estimated by applying the two packages (iWitness and Image Master Calib) and the corresponding differences.

Table 1. Calibration parameters and differences for the Nikon D80

	iWitness	***Image Master Calib***	***Difference***
c [mm]	*29.517*	*29.484*	*0.033*
xp [mm]	*11.896*	*11.922*	*-0.025*
yp [mm]	*7.823*	*7.836*	*-0.013*
K1	*1.45E-04*	*1.42E-04*	*2.57E-06*
K2	*-1.73E-07*	*-1.69E-07*	*-3.93E-09*
K3	*5.66E-11*		
P1	*-4.35E-06*	*-5.03E-07*	*-3.85E-06*
P2	*-3.00E-05*	*-3.02E-05*	*2.00E-07*

The Image Master Photo (Topcon, 2010b) was used to solve the bundle adjustment process and to extract the DSM. In order to avoid the local modification of the bed configuration, no targets were placed on the bed surface. Furthermore, because of the shape of the channel and the high banks, which made not easy the topographic survey, it was not possible to measure ground control points for the images orientation. The images orientation was calculated in an arbitrary reference system by applying a free-network solution bundle block adjustment and by using some calibrated bars to scale the photogrammetric model. This approach allows high precision measurements in close range photogrammetric surveys (Luhmann et al., 2006). In particular, 24 calibrated bars of known length (12 bars of 29 cm and 12 bars of 20 cm) were placed along the channel banks. Only twelve of the calibrated bars (7 of 29 cm and 5 of 20 cm) were used to scale the photogrammetric model; the remaining 12 bars (5 of 29 cm and 7 of 20 cm) were used to evaluate the accuracy of the bundle block adjustment. The difference of the distance between calculated from photogrammetric process and the calibrated distance (measured with a laboratory microscope with a precision of ±10 microns) represented the length measurement error (LME) which was calculated along with the root mean square error (RMSE) of all length measurements. This procedure was chosen in agreement with a German standard (VDI7VDE 2634 Part 1, 2002) for evaluation of object-space accuracy of three dimensional point measurement systems based on the LME.

Before to execute the bundle block adjustment it was necessary to fix the stereo pairs; we obtained 238 stereo pair in total. The tie points were collimated in semi-automatic way because the automatic triangulation (AT), generally used in aerial photogrammetry for automatic tie points measurement, have not provide acceptable results; for every stereo pair we measured a number of tie points variable in the range 6-9. All the tie points were detected on the surface of the channel; more than 700 tie points were measured.

The exterior orientation was performed using the camera calibration parameters calculated by applying both Image Master Calib and iWitness softwares. The results obtained by using the two

dataset were very similar. In particular, images coordinates residuals were less than one pixel, while the calibrated bars residuals used to scale the photogrammetric model were about few microns (root mean square error of ±0.006 mm for Image Master Calib dataset and of ±0.007 mm for iWitness dataset). Effective accuracy of the photogrammetric survey (LME) was obtained from the residuals of the calibrated bars not used in the bundle adjustment. Using Image Master Calib dataset, a root mean square error of ±0,372 mm was estimated, while by using iWitness dataset, the root mean square error was of ±0,365 mm.

The iWitness camera calibration parameters, which provided slightly better results, were used for the DSM extraction. It was necessary to resample all the stereoscopic pairs to obtain the corresponding epipolar images. The DSM of the meandering channel, reported in Figure 4, was calculated, with a step of 5 mm, by considering all the stereoscopic pairs. Because of the large number of the images (more than 300), almost several hours were necessary to obtain the complete DSM. The step of 5 mm was considered a good compromise between the level of detail required for the following analyses and the processing time. Finally, the total time (including the orientation and DSM extraction) required to obtain the detailed bed topography was almost some days. It should be noted that the orientation step required the major part of the time occurring for photogrammetric process. For this reason, the research is presently enlarged by reducing such a time interval of the processing phase for the same experimental and surveying conditions.

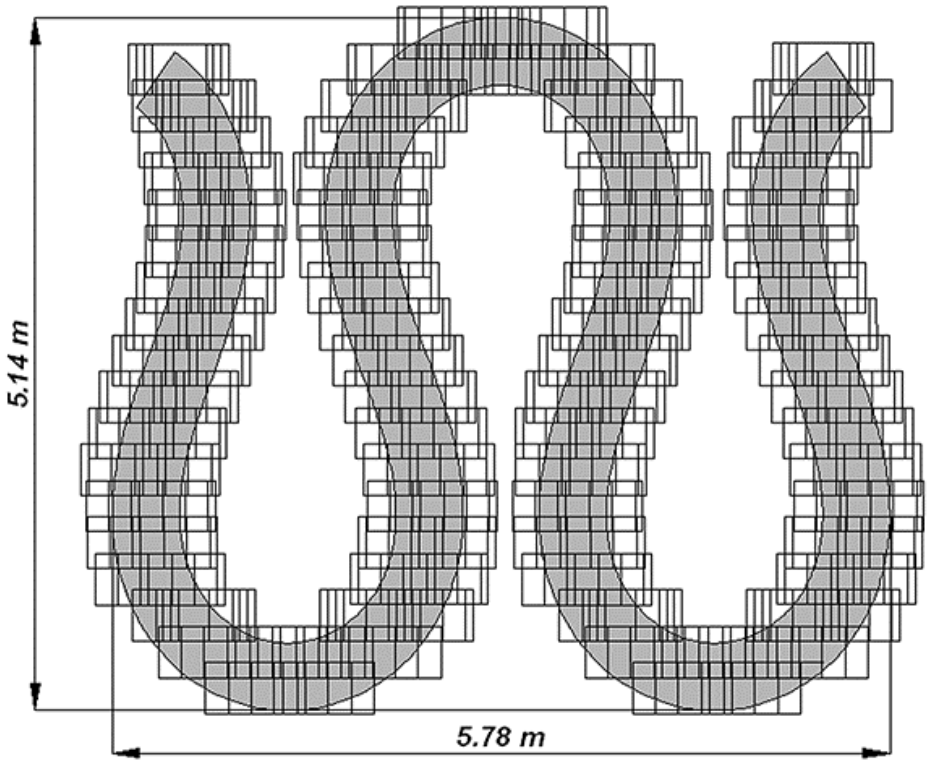

Figure 3. Photographic stereo coverage of the meandering channel

Figure 4. 3D view of the DSM of the meandering channel

FLOW PATTERN AND BED SHEAR STRESS DISTRIBUTION

Methods

In order to examine how the localization of the erosion zones on the bed could be related to flow and boundary shear stress distributions, the measured flow velocity data have been used to define peculiar maps of the cross-sectional and longitudinal flows and of shear velocity patterns along the meandering channel.

The flow velocity components were measured during another experimental run conducted with the hydraulic conditions described in section 2. and over the same bed surface surveyed with the photogrammetric technique. The measures were carried out by using the Acoustic Doppler Velocity Profiler (DOP 2000), based on Doppler effect. This instrument consists of a probe that is simultaneously emitter and receiver of acoustic pulses and it allows us to measure the instantaneous velocity profile along the probe's direction. Detailed measurements were conducted along the channel reach between sections 7 and 31 (Figure 1), by using three probes of emission frequency of 4 Mhz. During preliminary testing runs it was verified that such channel reach was less influenced by inflow and outflow conditions.

Details of measurement conditions (methods, measures accuracy, data sampling rate and acquisition time) can be found in Termini and Piraino (2011). The instantaneous transverse and vertical velocity components, $v_r(t)$ and $v_z(t)$, were measured at intervals of 1 cm; the instantaneous longitudinal component, $v_s(t)$, was measured along verticals spaces of 4 cm. Then, by using the instantaneous velocity components, the time-averaged flow velocity components (transversal, v_r, vertical, v_z, and longitudinal, v_s) have been determined in each measurement point.

RESULT AND DISCUSSION

Figures 5 and 6 report the vector representations of the transversal velocity component, v_r, and of the vertical velocity component, v_z, at the characteristic sections 7, 10, 13, 16, 19. It should be noted

that only meander wave between sections 7 and 19 (i.e. between two consecutive crossover sections) has been represented in these figures, taking into account that, as several literature studies show (among others Hooke, 1975; Whiting and Dietrich, 1993; da Silva et al., 2006; Termini, 2009; Binns and Da Silva, 2009), similar behaviour can be observed between the two consecutive crossover sections downstream (i.e., for the considered case, between sections 19 and 31). For the specific case examined, this behavior has been also confirmed by analyses reported in previous works (see as an example in Termini, 2009 and in Termini and Piraino, 2011).

From Figure 5 it can be observed that, because of the local bed deformation, at the inflection section 7 all vectors v_r are directed toward the inner bank (negative versus) both near the inner-bank and in the central region, with exception of a thin area of the central region where the vectors change the sign near the bed. Near the outer-bank, all vectors v_r are directed toward the outer bank (positive versus), probably because of the influence of the inflow conditions. As the channel curvature increases (section 10), at the entrance of the curve, all v_r vectors are directed toward the outer bank (positive versus) while, at the bend apex (section 13), v_r changes again sign within the section. In fact, both near the inner-bank, where deposition occurs, and in the major part of the central-region, all vectors assume negative versus (i.e. are directed toward the inner-bank). Moving towards the outer-bank, where erosion occurs, the vectors v_r are directed positively near the free surface while near the bed they are directed toward the inner bank. As the channel curvature decreases, i.e. passing from section 13 to section 16, the crossed vertical profiles of v_r are found both in the central region and very close to the outer bank. Finally, at the inflection section downstream (section 19) the radial velocity vectors are all directed toward the inner bank. Thus, as the channel curvature increases, crossed vertical profiles of v_r occur near the outer bank.

From Figure 6 it can be observed that at the inflection section 7 all vectors v_z are directed toward the bed (negative versus); in section 10 (i.e. at the entrance of the bend) v_z assumes in general negative sign (toward the bed), both near the inner-bank and in central region, although in some thin areas v_z changes the sign; near the outer-bank the vectors v_z are all directed toward the free surface (positive sign) with exception of a thin area near the free-surface where they are negative. At apex section 13, in the major part of the central-region, and partially near the outer-bank, the vectors v_z change the versus passing from the free-surface (where the versus is negative) to the bed (where the versus is positive). As the channel curvature decreases (section 16), the crossed vertical profiles of v_z especially occur near the outer-bank. Finally, in the inflection section downstream (section 19), all vectors v_z are directed toward the bed (negative versus), except in part of the central region and near the outer-bank where they become positive (toward the free-surface) near the bed. It can be concluded that, also for v_z crossed vertical profiles can be observed near the outer bank, where erosion occur.

The effect of the momentum transport of cross-sectional motion on the downstream velocity restistribution can be examined through Figure 7. This figure shows the distribution of the depth-averaged longitudinal flow velocity, $\overline{v_s}$, along the channel reach considered. This figure highlights that the maximum $\overline{v_s}$ lies, at the bend entrance, near the inner bank. Then, it moves towards the outer bank. Along the channel reach 10 – 13 (and along the channel reach 22 – 25) the maximum of $\overline{v_s}$ further shifts towards the outer bank but it maintains at a certain distance from the outer bank itself. This is due to the presence of counter-rotating circulation motion near the outer bank, as observed by Termini and Piraino (2011). Passing from section 13 to section 16 (and from section 25 to section 28)**,** the maximum of $\overline{v_s}$ tends to slightly move towards the central region of the cross-section. Then, along the reach 16-19 (and along the reach 28-31), the $\overline{v_s}$ decreases in value and the maximum is found at the outer bank.

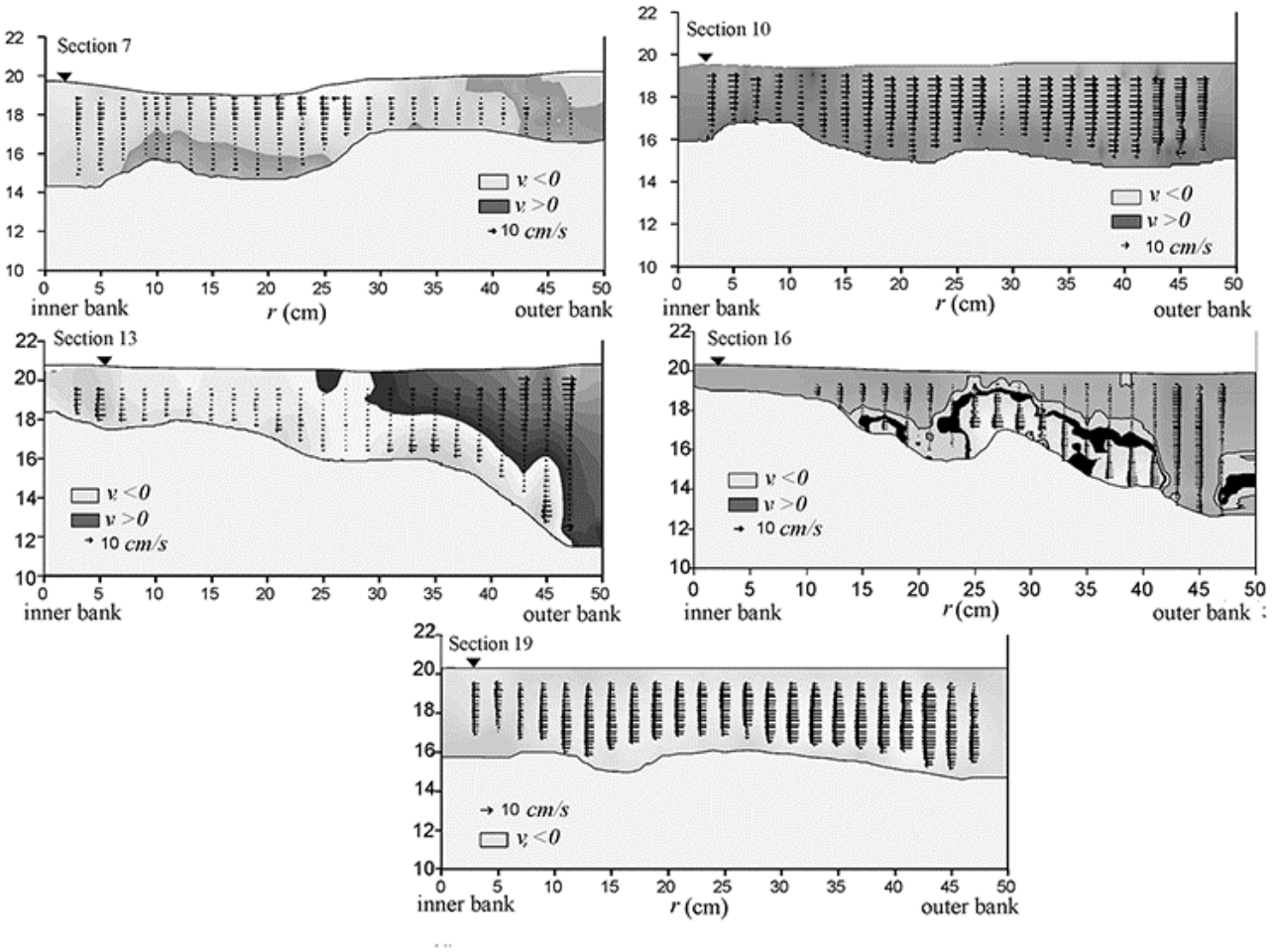

Figure 5. Vector representation of transversal flow velocity component at characteristic sections

This behaviour confirms that, in accordance with Blanckaert ad Graf (2001), the advective momentum transport by the cross-circulation plays an important role on the bed and outer bank erosion and, thus, on the meander wave morphological evolution. This further highlights the importance of the accurate identification of the cross-circulation effect. But, this identification is strongly related to the accurate identification of the bed topography (and, thus, of the water depths) which, in turn, depends on the redistribution of downstream velocity and of bed shear stress due to the advective momentum transport by the cross-circulation itself.

In order to understand the aforementioned effects on the distribution of the boundary shear stress $\tau_b = \rho u_*^2$ (with ρ= water density; u_* = shear velocity), the values of the local shear velocity, u_*, have been determined along the examined channel reach. Thus, the longitudinal velocities near the bed (z/h<= 0.2) (Whiting and Dietrich, 1991; Nezu and Nakagawa, 1993) have been interpolated by the logarithmic law of the wall, by imposing the minimization of the mean square errors between measured and calculated longitudinal flow velocities and assuming the shear velocity as the unknown parameter. In Figure 8 the distribution of the shear flow velocity along the channel reach 7-31 is compared with the obtained bed topography. This figure confirms the existence of the strong interaction between the examined flow pattern, which determines the bed shear stress distribution along the channel, and the bed deformation. It can be observed, in fact, that the higher values of the shear velocity are found in correspondence to the erosion zones identified along the channel reach considered.

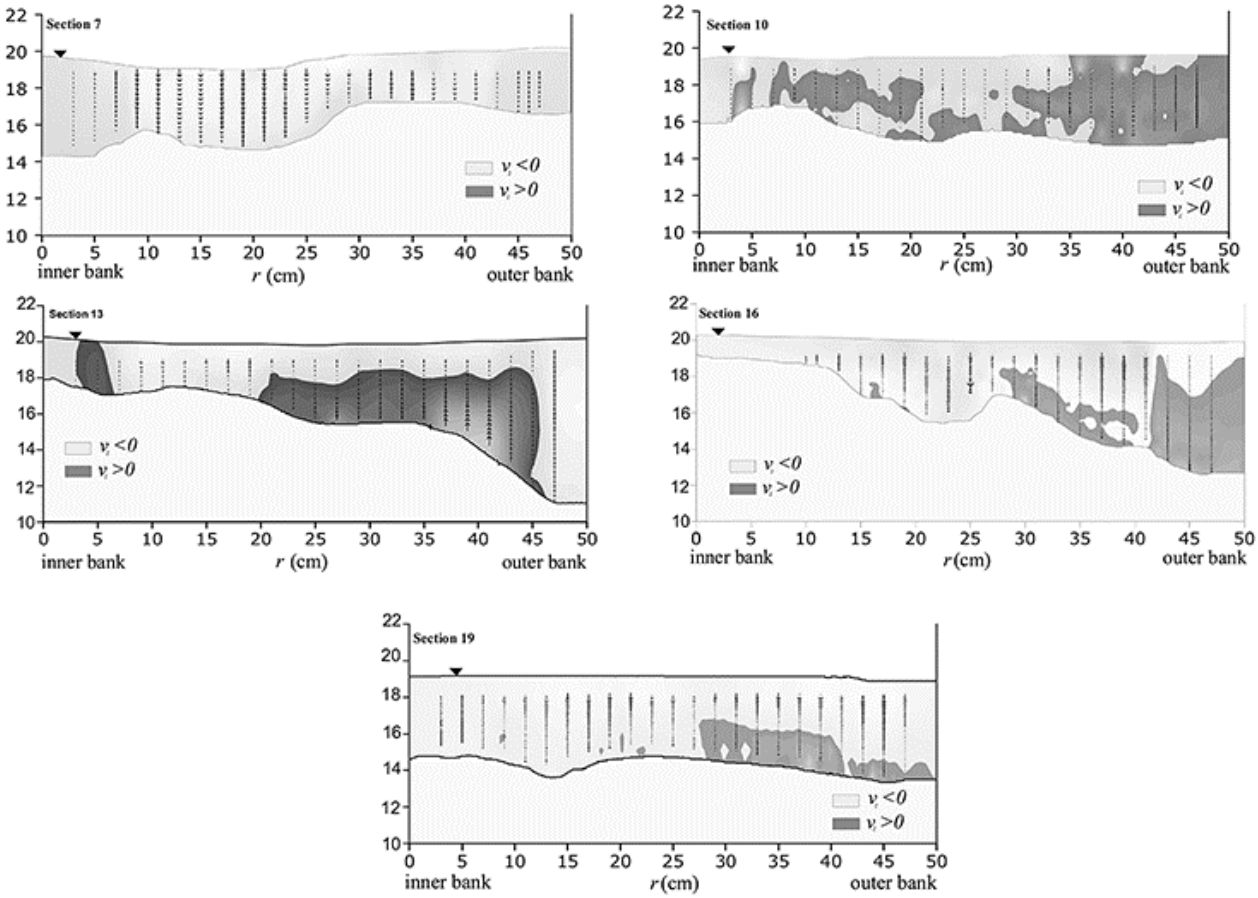

Figure 6. Vector representation of vertical flow velocity component at characteristic sections

A general conclusion from the aforementioned is that high resolution topographic data play an important role in prediction of flow-bed-banks interaction processes.

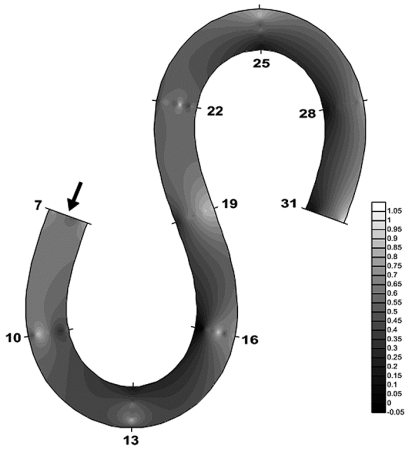

Figure 7. Map contours (channel reach between sections 7 and 19) of depth-averaged longitudinal flow velocity $\overline{v_s}$ (m/s)

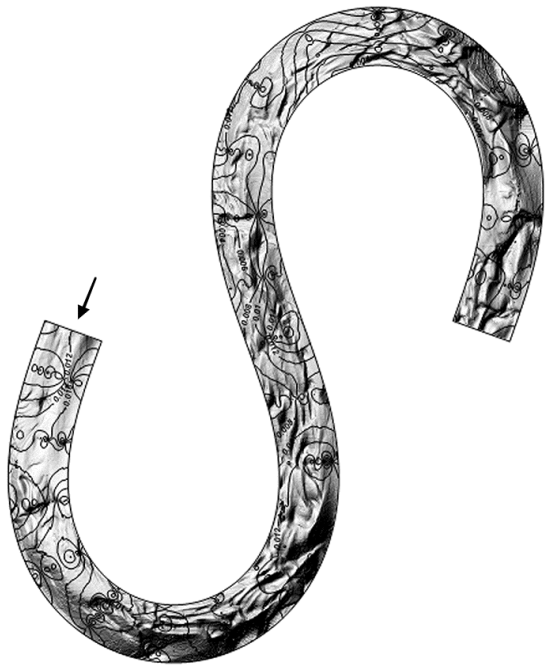

Figure 8. Comparison between the DSM and the contour-lines of shear flow velocity, u_* (m/s), along the channel reach between sections 7 and 31

CONCLUSION

The analysis of basic mechanisms of flow-bed interactions, useful for forecasting models, is often conducted in laboratory flumes. For this purpose, rapid and accurate devices for recording bed topography are needed.

In the last decades, geoinformatics technologies have determined a transformation in the way of surveying morphological changes in rivers, allowing the rapid topographic surface measurement and a high-quality acquisition of the surface itself. Laser scanning technology are more often used for medium-scale and small-scale applications. But, for large-scale applications (as well as in laboratory flumes) digital photogrammetry is still today preferred.

According with Chandler et al. (2007), digital photogrammetry is unique for its flexibility of scale and for the ability to extract automatically very dense DSM with an accuracy and a level of detail similar, or equal, to that achieved by laser scanner device. But, the main disadvantage of photogrammetry is related to the time required for the images orientation, especially in the case of very huge photogrammetric block. In fact, the automation of the images orientation in close range applications is still an open topic in photogrammetry.

In this paper a photogrammetric survey with a non-metric digital camera has been applied to measure the equilibrium bed topography of a large amplitude meandering laboratory flume (≅ 27 m long). The non-metric camera was calibrated by using two commercial softwares and two different calibration dataset. The image acquisition time was approximately equal to 2 hours, which can be considered short taking into account the large number of images (more than 300). This was possible because the camera was firmly mounted on a 3D automatic position system which allowed the surveying procedure to be semi-automatic. Due to the large number of images and to the complex

shape of the channel it was necessary to measure more than 700 tie points for the images orientation; no ground control points were used in images orientation but only some scale bar to scale the photogrammetric model. The accuracy of the photogrammetric survey was computed through the root mean square error (RMSE) of the length measurement error (LME) for some scale bar used as check. A very high accuracy (root mean square error of about +/-0,3 mm), compatible with the accuracy (+/-0.5 mm) required for the application, was obtained.

Thus, a detailed DSM (step of 5 mm) of the meandering channel has been determined. The images orientation step required almost 5 days while almost one day was necessary to obtain the complete DSM. Thus, the orientation step required the major part of the time occurring for photogrammetric process. For this reason, further applications will be conducted in order to reduce such a time interval of the processing phase for the same experimental and surveying conditions.

In order to verify the importance of the high resolution DSM in investigating flow-bed interaction processes, the obtained bed surface has been compared with peculiar maps showing the flow velocity pattern and the resulting shear velocity distribution. Such maps have been obtained by using detailed data on the 3D flow field, previously measured by a high-precision acoustic profiler.

The comparison has demonstrated that the accurate identification of the mean flow velocity redistribution is strongly related to the accurate identification of the bed topography, which is mainly shaped by the bed shear stress distribution (see as an example in Hooke, 1975; Whiting and Dietrich, 1993). It has been observed that the localization of the erosion zones on the bed is approximately coincident with the localization of the zones of higher values of the shear velocity.

This work thus highlights the need of high resolution topographic data in prediction of flow-bed-banks interaction processes verifying the applicability of close range photogrammetry as automatic surveying procedure in order to obtain the DSM of the examined laboratory flume with a good compromise between the high accuracy and the surveying time required.

It should be emphasized that, for the specific purposes of the work, the presented experimental results come from measurements collected during a single run, i.e. for a single value of flow discharge. More analyses on flow patterns and bed deformation for different values of flow discharge can be found in previous works (Termini and Piraino, 2011). The experimental research is presently enlarged by examining the effect of the variation of other input parameters (flow discharge, bed roughness and the non-uniformity of sediments), on the flow-bed deformation interplay.

REFERENCES

[1]. Abd-Elrahman, A., Gad-Elraab, M., **2008**. Using commercial-grade digital camera images in the estimation of hydraulic flume bed changes: case study. Surveying and Land Information Science, 68(1), 35-45.

[2]. Binns A.D., da Silva A.M.F., **2009**. On the quantification of the bed development time of alluvial meandering streams. Journal of Hydraulic Enginnering, 135(5), 350-360.

[3]. Blanckaert, K., Graf, W.H. **2001**. Mean Flow and Turbulence in Open-channel Bend. Journal of Hydraulic Engineering;127(10), 835-847.

[4]. Blanckaert, K., Graf, W.H., **2004**. Momentum transport in sharp open-channel bends. Journal of Hydraulic Engineering;130(3), 186-198.

[5]. Blanckaert, K., Bushman F.A., Shielen R. Ad Wijbenga J.H.A., **2008**. Redistirbution of velocity and Bed-shear stress in straight and curved open channels by means of a bubble screen: laboratory experiments. Journal of Hydraulic Engineering;134(2), 186-198.

[6]. Bridge, J., Jarvis, J., **1976**. Flow and Sedimentary Processes in The Meandering River South Eskglenclova, Scotland. Earth surface processes, 1, 303-336.

[7]. Chandler, J.H., Shiono, K., Rameshwaren, P., Lane S.N., **2001**. Measuring flume surfaces for hydraulics research using a Kodak DSC460. Photogrammetric Record, 17(97), 39-61.
[8]. Chandler, J.H., Buffin-Belanger, T., Rice, S., Reid, I., Graham, D.J., **2003**. The accuracy of a river bed moulding/casting system and the effectiveness of a low-cost digital camera for recording river bed fabric. Photogrammetric Record, 18(103), 209-223.
[9]. Chandler, J.H., Fryer, J.G., Jack, A., **2005**. Metric capabilities of low-cost digital cameras for close range surface measurement. The Photogrammetric Record, 20(109), 12-26.
[10]. Chandler, J.H., Lane S.N., Walstra J., **2007**. Quantifying landform change. In Applications of 3D measurement from images. J. Fryer, H. Mitchell and J. Chandler. Whittles Publishing.
[11]. Chang, H.H., **1988**. Fluvial Processes in River Engineering. Wiley-Inter-science publication - John Wiley and Sons.
[12]. Cochrame, T.A., Flanagan, D.C., **2006**. Sediment deposition in simulated rill under shallow flow conditions. Transactions of the American Society of Agricultural and Biological Engineers, 49(4), 893-903.
[13]. Da Silva, A.M.F., El-Tahawy, T., Tape W.D., **2006**. Variations of flow pattern with sinuosity in sine-generated meandering streams. Journal of Hydraulic Enginnering, 132(10), 1003-1014.
[14]. Dietrich, W.E., Smith, D. **1983**. Influence of the Point Bar on Flow Through Curved Channels, Water Resources Research, 19(5), 1173-1192.
[15]. Friedrichs, M., Graf, G., **2006**. Description of a flume channel profilometry tool using laser line scans. Aquatic Ecology, 40(4), 493-501.
[16]. Gessese, D., Fuchs, H., Mansberger, R., Klik, A., Rieke-Zapp, D., **2010**. Assessment of erosion, deposition and rill development on irregular soil surfaces using close range digital photogrammetry. The Photogrammetric Record, 25(131), 299-318.
[17].Heng, B.C.P., Clander, J.H., Armstrong, A., **2010**. Applying close range digital photogrammetry in soil erosion studies. The Photogrammetric Record, 25(131), 240-265.
[18]. Hickin E. J., Nanson G., **1984**. Lateral migration rates of river bends. Journal of Hydraulic Engineering, ASCE, 110(4),1557-1567.
[19]. Hooke, R.L., **1975**. Distribution of sediment transport and shear stress in a meander bend. Journal of Geology, 83, 543-565.
[20]. Hooke J., **2003**. River meander behavior and instability: a framework for analysis. Transactions of the Institute of British Geographers, 28(2), 238-253.
[21]. Kraus K., **1999**. Photogrammetry, Fundamentals and Standard Processes, Volume 1, 1999, 4th edition, Dümmler/Bonn.

[22]. Langbein, W.B., Leopold, L.B. **1966**. River meanders-theory of minimum variance. U.S. Geology Survey Professional, paper n. 422 (H), H1-H15.

[23]. Lane, S.N., Westaway, R.M., Hicks, D.M. **2003**. Estimation of erosion and deposition volumes in a large, gravel-bed, braided tiver using synoptic remote sensing. Earth Surface Processes and Landforms. 28, 249-271.

[24]. Lanzoni S., Seminara G., **2006**. On the nature of meander instability. Journal of Geophysical Research, vol. III, F04006, doi: 10.1029/2005JF000416.

[25]. Luhmann T., Robson S., Kyle S., Harley I., **2006**. Close Range Photogrammetry. Principles, Methods and Application. Whittles Publishing.
[26]. Nezu I., Nakagawa H., **1993**, Turbulence on open channel flows, A.A. Balkema Publishers, Rotterdam, the Netherlands.